Secondary Phases in (001)$RBa_2Cu_3O_{7-\delta}$ Epitaxial Thin Films

S. V. Samoylenkov,* O. Yu. Gorbenko, I. E. Graboy, A. R. Kaul, H. W. Zandbergen,† and E. Connolly†

Department of Chemistry, Moscow State University, 119899 Moscow, Russia, and National Centre for HREM, Laboratory of Materials Science, Delft University of Technology, Rotterdamseweg 137, 2628 AL Delft, The Netherlands

Received February 10, 1999. Revised Manuscript Received June 10, 1999

The composition and orientation of secondary phases in epitaxial (001)$RBa_2Cu_3O_{7-\delta}$ thin films grown by MOCVD were investigated by HREM, XRD, SEM, and other techniques. The observed secondary phases often did not correspond to those expected from equilibrium phase diagrams of bulk R−Ba−Cu−O systems. No evidence was found for the presence of R_2BaCuO_5 or $BaCuO_2$, which are the equilibrium phases with bulk $RBa_2Cu_3O_{7-\delta}$. In contrast, inclusions of well-oriented R_2CuO_4 (R = Gd), R_2O_3 (R = Lu, Ho, Y), $R_2Cu_2O_5$ (R = Lu), Ba_2CuO_3, and $BaCu_3O_4$ were observed, depending on the films' stoichiometry. It is concluded that the formation of coherent or semicoherent interfaces between embedded inclusions and the surrounding matrix is critical for a stabilization of otherwise nonequilibrium oxide phases in epitaxial films. The crystal structure of unstable-in-bulk cuprate $BaCu_3O_4$ was determined using electron nanodiffraction of the films' cross sections.

I. Introduction

Understanding the processes governing the formation of secondary phases in $RBa_2Cu_3O_{7-\delta}$ epitaxial thin films, where R is a rare earth element, is an important task from the point of view of both fundamental science and high T_c superconducting device applications. The composition, orientation, and size of secondary phase inclusions in epitaxial $RBa_2Cu_3O_{7-\delta}$ films depend on a complicated interplay of systems thermodynamics, growth kinetics, and structure and lattice parameters of the substrate material. To understand clearly the processes that lead to the formation of particular secondary phases, all these aspects should be taken into account. Much effort has been made to elucidate the influence of stoichiometry on phase composition and the resulting superconducting properties of $RBa_2Cu_3O_{7-\delta}$ films, especially when R = Y.[1−5] However, these results are often difficult to compare with each other because of the variety of deposition conditions and growth techniques used in research.

The equilibrium thermodynamics of R−Ba−Cu−O systems, as well as of related subsystems, has been extensively explored since superconductivity at ca. 90 K in $RBa_2Cu_3O_{7-\delta}$ compounds[6] was discovered.[7−19] If $r(R^{3+})$ is larger than some critical value—the threshold is believed to occur around $r(Gd^{3+})$—$R_{1+x}Ba_{2-x}Cu_3O_{7-\delta}$ solid solutions may form. The range of x variation depends on the ionic radius of R^{3+}, $r(R^{3+})$, temperature, and partial oxygen pressure, $p(O_2)$[12,13,19] (Figure 1). $RBa_2Cu_3O_{7-\delta}$ with $r(R^{3+})$ smaller than that of gadolinium, possess no significant cation nonstoichiometry under equilibrium conditions.[7−11,15,19] Consequently, even small deviations of sample stoichiometry from the ideal 1:2:3 ratio may lead to the appearance of secondary phases. On the other hand, minor fluctuations of the composition of deposited layers are inherent in film growth of $RBa_2Cu_3O_{7-\delta}$ by routine methods such as laser ablation,[20] metalorganic chemical vapor deposition (MOCVD),[21] magnetron sputtering,[22] and other techniques, owing to various reasons.

† Delft University of Technology.
* Corresponding author. E-mail: sergej@iopwws4.iopw.ing.tu-bs.de.

(1) Carlson, D. J.; Siegal, M. P.; Phillips, J. M.; Tiefel, T. H.; Marshall, J. H. *J. Mater. Res.* **1990**, *5*, 2797.
(2) Waffenschmidt, E.; Waffenschmidt, K. H.; Arndt, F.; Boeke, E.; Musolf, J.; He, X.; Heuken, M.; Heime, K. *J. Appl. Phys.* **1994**, *75*, 4092.
(3) Baudendacher, F.; Hirata, K.; Berberich, P.; Kinder, H.; Assmann, W. In *High T_c Superconducting Thin Films*, Correra, L., Ed.; Elsevier Science: Amsterdam, 1992; p 365.
(4) Grigis, Ch.; Schamm, S. *Ultramicroscopy* **1998**, *74*, 159.
(5) Doudkowsky, M.; Santiso, J.; Berton, S.; Figueras, A.; Bassas, J. *Physica C* **1997**, *288*, 1.
(6) Wu, M. K.; Ashburn, J. R.; Torng, C. J.; Hor, P. H.; Meng, R. L.; Gao, L.; Huang, Z. J.; Wang, Y. Q.; Chu, C. W. *Phys. Rev. Lett.* **1987**, *58*, 908.
(7) Ahn, B. T.; Lee, V. Y.; Beyers, R.; Gur, T. M.; Haggins, R. A. *Physica C* **1990**, *167*, 529.
(8) Voronin, G. F.; Degterov, S. A. *Physica C* **1991**, *176*, 387.
(9) Voronin, G. F.; Degterov, S. A. *J. Solid State Chem.* **1994**, *110*, 50.
(10) Brosha, E. L.; Garzon, F. H.; Raistrick, I. D. *J. Am. Ceram. Soc.* **1995**, *78*, 1745.
(11) Hauck, J. *Supercond. Sci. Technol.* **1996**, *9*, 1033.
(12) Wu, H.; Kramer, M. J.; Dennis, K. W.; McCallum, R. W. *Physica C* **1997**, *290*, 252.
(13) Park, M.; Kramer, M. J.; Dennis, K. W.; McCallum, R. W. *Physica C* **1996**, *259*, 43.
(14) Czerwonka, J.; Eick, H. A. *J. Solid State Chem.* **1991**, *90*, 69.
(15) Oniyama, E.; Wahlbeck, P. G.; Peterson, D. E.; Coulter, J. Y.; Peterson, E. J. *Physica C* **1997**, *288*, 151.
(16) Lindemer, T. B.; Specht, E. D. *Physica C* **1995**, *255*, 81.
(17) Subasri, R.; Pankajavalli, R.; Sreedharan, O. M. *Physica C* **1997**, *281*, 85.
(18) Kale, G. M.; *J. Solid State Chem.* **1996**, *125*, 13.
(19) Wong-Ng, W.; Paretzkin, B.; Fuller, E. R. *J. Solid State Chem.* **1990**, *85*, 117.
(20) Gong, J. P.; Kawasaki, M.; Fujito, K.; Tsuchiya, R.; Yoshimoto, M.; Koinuma, H. *Phys. Rev. B* **1994**, *50*, 3280.

10.1021/cm991016v CCC: $18.00
Published on Web 08/07/1999

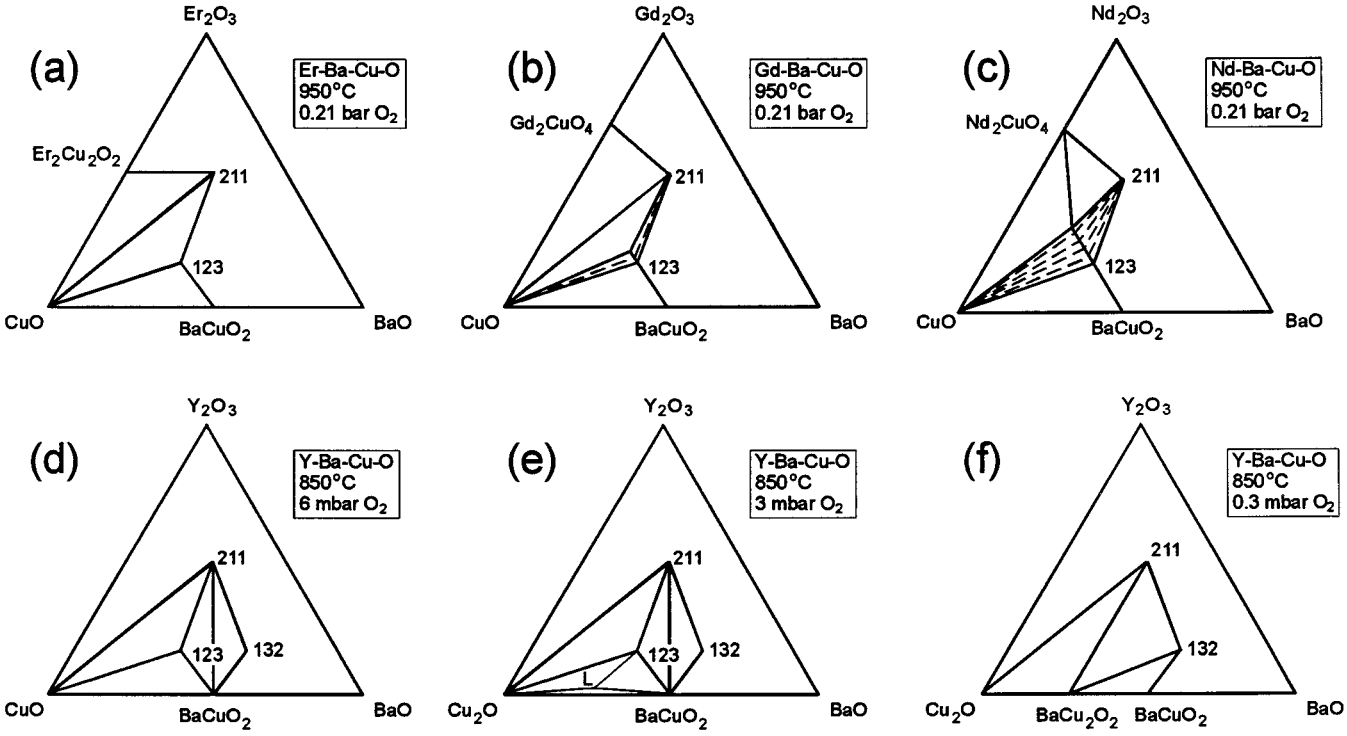

Figure 1. Equilibrium phase relations in the copper-rich part of the $R_2O_3-BaO-CuO(Cu_2O)$ triangle for various R^{3+} and $p(O_2)-T$ conditions. 123, $RBa_2Cu_3O_{7-\delta}$; 132, $RBa_3Cu_2O_x$; 211, R_2BaCuO_5. The data of Wong-Ng et al.[19] (a−c) and Ahn et al.[7] (d−f).

Due to the use of relatively low temperatures and $p(O_2)$ values in thin film synthesis, the thermodynamics and kinetics of phase formation in thin films differ from those of bulk ceramics. Off-stoichiometry components can be incorporated into the structure of growing $RBa_2Cu_3O_{7-\delta}$ films as structural defects, provided the kinetics of the phase formation is slow in comparison with the deposition rate.[20] For example, the formation of cubic perovskite $(Y,Ba)CuO_{3-x}$ with a significant cation disorder in the Y and Ba crystallographic positions and/or Y for Ba substitution was observed by XRD, if the film growth was carried out at reduced deposition temperatures.[23−25] Too high deposition temperatures and/or too low deposition $p(O_2)$ values may also be the reason for R/Ba cation disorder as well as related crystallographic vacancies, mainly in the apical oxygen site.[25,26] In this case, $p(O_2)-T$ deposition conditions approach the instability border of $RBa_2Cu_3O_{7-\delta}$, or even lie outside the area of thermodynamic stability.[25,26] Apart from point defects and substitution, off-stoichiometry cations may also be incorporated into the film structure due to the formation of extended defects,[27] such as $Y_2Ba_4Cu_7O_{15-\delta}$ or $YBa_2Cu_4O_8$ structural fragments,[28] anti-phase boundaries, and stacking faults.[28−30] The optimal $p(O_2)-T$ growth conditions, with respect to the films' structural quality and superconducting properties, have often been reported to be located near the equilibrium line between CuO and Cu_2O oxides.[31,32]

Some secondary phase inclusions tend to appear in epitaxial $RBa_2Cu_3O_{7-\delta}$ films being well oriented with respect to $RBa_2Cu_3O_{7-\delta}$ structure. Thus, semicoherent nanoinclusions of Y_2O_3 have been observed by HREM in (001)$YBa_2Cu_3O_{7-\delta}$ epitaxial films enriched with yttrium.[33−36] This fact is astonishing, taking into account that the Y_2BaCuO_5 phase, not Y_2O_3, is the yttrium-rich phase which exists in equilibrium with the $YBa_2Cu_3O_{7-\delta}$ compound. Nevertheless, the formation of Y_2BaCuO_5 inclusions in epitaxial (001)$YBa_2Cu_3O_{7-\delta}$ films is actually quite uncommon. Due to epitaxy, the nature of precipitating secondary phases is distinctly influenced by the substrate orientation.[37] It has been shown that Y_2O_3 inclusions form in films grown on (001)MgO substrates, while on (110)MgO substrates the typical inclusions were Y_2BaCuO_5 particles.[37] By means of in situ RHEED analysis of MBE film growth, Locquet

(21) Samoylenkov, S. V.; Gorbenko, O. Yu.; Kaul, A. R.; Rebane, Ya. A.; Svetchnikov, V. L.; Zandbergen, H. W. *J. Alloys Compd*. **1997**, *251*, 342.
(22) Han, Z.; Selinder, T. I.; Helmersson, U. *J. Appl. Phys*. **1994**, *75*, 2020.
(23) Agostnelli, J. A.; Chen, S.; Braunstein, G. *Phys. Rev. B* **1991**, *43*, 11396.
(24) Ye, J.; Nakamura, K. *Phys. Rev. B* **1994**, *50*, 7099.
(25) McManus-Driscoll, J. L.; Alonso, J. A.; Wang, P. C.; Geballe, T. H.; Bravman, J. C. *Physica C* **1994**, *232*, 288.
(26) Aswal, D. K.; Gupta, S. K.; Narang, S. N.; Sabharval, S. C.; Gupta, M. K. *Thin Solid Films* **1997**, *292*, 277.
(27) Fendorf, M.; Tidjani, M. E.; Burmester, C. P.; Wille, L. T.; Gronsky, R. In *High T_c Superconducting Thin Films*, Correra, L., Ed.; Elsevier Science: Amsterdam, 1992; p 771.
(28) Wang, Z. L.; Lowndes, D. H.; Christen, D. K.; Kroeger, D. M.; Klabunde, C. E.; Norton, D. P. *Physica C* **1995**, *252*, 125.
(29) Blank, D. H. A.; Bijlsma, M. E.; Moerman, R.; Rogalla, H.; Stork, F. J. B.; Roshko, A. *J. Alloys Compd*. **1997**, *251*, 27.
(30) Takeno, S.; Nakamura, S.; Sagoi, M.; Miura, T. *Physica C* **1991**, *176*, 151.
(31) Chambonnet, D.; Fages, C.; Belouet, C.; Moriceau, H.; Schwerdtfeger, M.; Villegier, J. C.; Keller, D. *J. Alloys Compd*. **1993**, *195*, 243.
(32) Yamane, H.; Hasei, M.; Kurosawa, H.; Hirai, T.; Watanabe, K.; Kobayashi, N.; Muto, Y. In *High T_c Superconducting Thin Films*; Correra, L., Ed.; Elsevier Science: Amsterdam, 1992; p 319.
(33) Selinder, T. I.; Helmersson, U.; Han, Z.; Sundgren, J.-E.; Sjöström, H.; Wallenberg, L. R. *Physica C* **1992**, *202*, 69.
(34) Dorignac, D.; Schamm, S.; Grigis, C.; Sévely, J.; Santisto, J. Figueras, A. *Physica C* **1994**, *235−240*, 617.
(35) Verbist, K.; Vasiliev, A. L.; van Tendeloo, G. *Appl. Phys. Lett*. **1995**, *66*, 1424.
(36) Selinder, T. I.; Helmersson, U.; Han, Z.; Wallenberg, L. R. *Thin Solid Films* **1993**, *229*, 237.
(37) Broussard, P. R.; Wall, M. A.; Talvacchio, J. *J. Mater. Res*. **1998**, *13*, 954.

et al.[38] observed the nucleation of Cu_2O particles on the surface of (001)$DyBa_2Cu_3O_{7-\delta}$ films grown on a (001)-$SrTiO_3$ substrate, though CuO formed on bare (001)-$SrTiO_3$ or (001)MgO substrate surfaces under the same $p(O_2)-T$ conditions. It was proposed that the terminating surface layer of a (001)$DyBa_2Cu_3O_{7-\delta}$ film (either $CuO_{1-\delta}$ or BaO) favors the nucleation of Cu_2O oxide with a cubic structure at the expense of the monoclinic CuO phase.

Epitaxial film growth can assist formation of phases whose bulk synthesis is difficult due to kinetic limitations of solid-state reactions. The synthesis of single phase (001)$RBa_2Cu_3O_{7-\delta}$ epitaxial films with R = $Lu_{1-x}Tb_x$, $Th_{1-x}Ca_x$,[39] and $Pr_{1-x}Ca_x$[40] has been reported. In these solid solutions the single phase region of the x coefficient is remarkably wider for thin films than for bulk materials.

Summarizing all these considerations, three possible explanations for the appearance of "unusual" secondary phases in epitaxial (001)$RBa_2Cu_3O_{7-\delta}$ films may be outlined:

(a) Nucleation of nanoparticles of a secondary phase takes place in the MOCVD gas phase and the growing film incorporates the particles formed. Further chemical interaction between the buried particle and the film matrix is hindered due to kinetical reasons, so that thermodynamic equilibrium cannot be reached.

(b) Equilibrium phase relations in R−Ba−Cu−O systems under the conditions routinely used in thin film growth differ from those known for bulk ceramics. In this case, the secondary phases observed are actually in thermodynamic equilibrium with $RBa_2Cu_3O_{7-\delta}$.

(c) Perfect orientation of secondary phase inclusion with respect to the $RBa_2Cu_3O_{7-\delta}$ film matrix and/or the single crystalline substrate may provide a substantial decrease in its free energy due to the formation of coherent grain boundaries if the inclusions dimensions are small. The stability of an inclusion in an epitaxial film matrix is therefore influenced by its crystal structure and its orientation, along with thermodynamical constants of the bulk. Depending on the size of the inclusion, this case may correspond either to a thermodynamic equilibrium or to a metastable state.

In this paper we report on HREM and XRD studies of secondary phases in (001)$RBa_2Cu_3O_{7-\delta}$ (R = Lu, Ho, Y, Gd) epitaxial thin films prepared by MOCVD. Films of Ba−Cu−O system on perovskite single crystalline substrates were studied as well. Special attention is paid to the appearance of nonequilibrium phases, and to the dependence of secondary phase composition on rare earth cation. Our results demonstrate the important role of the inclusions' structure and orientation in stabilizing particular secondary phases in $RBa_2Cu_3O_{7-\delta}$ films and rule out the first two of the explanations given above.

II. Experimental Section

Thin Film Preparation. (001)$RBa_2Cu_3O_{7-\delta}$ (R = Lu, Ho, Y, Gd) and Ba−Cu−O thin films were grown on single crystalline substrates by MOCVD as described elsewhere.[41,42] The deposition temperature was varied between 800 and 835 °C and the oxygen partial pressure, $p(O_2)$, was chosen in the interval 1.7−2.5 mbar. The typical growth rate was about 0.4 μm/h. Unless otherwise stated, all films were cooled under oxygen flow, with an intermediate annealing at 450 °C for 1 h. Dipivaloylmethanates $M(thd)_n$ were used as volatile precursors for all metals, except for barium, for which the adduct with *o*-phenanthroline, $Ba(thd)_2$·2Phen, was used.

Table 1. Optimum MOCVD Deposition Conditions Found, Typical Superconducting Characteristics, and *c* Lattice Parameters of 0.3 μm Thick Epitaxial (001)$RBa_2Cu_3O_{7-\delta}$/$LaAlO_3$ Films

R	$r(R^{3+})$, Å (ref 50)	T_{dep}, °C	$p(O_2)_{dep}$, mbar	T_c, K[a]	j_c(77K,0T), 10^6 A/cm^2 [a]	c, Å[a]
Lu	0.977	800	1.3	88	2.7	11.670(5)
Ho	1.015	820	1.7	90	2.5	11.690(5)
Y	1.018	820	1.7	90	2.0	11.690(5)
Gd	1.053	835	2.5	91	1.0	11.710(5)

[a] For the fully oxygenated films.

Characterization. X-ray diffraction analysis was carried out in various geometries using SIEMENS D5000 and DRON 3M diffractometers. SEM and EDX analyses of the film compositions were performed using a CAMSCAN electron microscope. Superconducting characteristics of $RBa_2Cu_3O_{7-\delta}$ films were derived from ac magnetic measurements.

TEM/HREM Experiments and the Electron Diffraction. Cross sectional electron transparent areas of (001)$RBa_2Cu_3O_{7-\delta}$ films were obtained by ion milling, with the film facing away from the ion gun. Electron microscopy was performed using a Philips CM30UT electron microscope equipped with the field emission gun operating at 300 kV, and a Link EDX element analysis system. Electron diffraction was performed with spot sizes between 4 and 20 nm; exposure times ranged from 0.1 to 5 s. To reduce the electron microscope induced contamination and amorphization, the specimens were cooled to about 100 K. Structural refinements were performed using the MSLS software package,[43−45] which takes dynamic diffraction fully into account. Apart from parameters related to the crystal structure, some additional parameters, such as absorption factor, crystal thickness, and orientation, had to be refined simultaneously. The standard deviations of refined crystallographic positions of $BaCu_3O_4$, given in brackets in Table 2, are based on the refinement statistics, and consequently experimental errors are not included.

III. Results

Characteristics of (001)$RBa_2Cu_3O_{7-\delta}$ Epitaxial Thin Films Grown under Optimized Conditions. Typical characteristics of epitaxial (001)$RBa_2Cu_3O_{7-\delta}$/$LaAlO_3$ thin films prepared are presented in Table 1. The optimum conditions followed the $p(O_2)-T$ line of $CuO \Leftrightarrow Cu_2O + {}^1/_2O_2$ equilibrium[16] rather well, in agreement with previous observations.[31,32] The optimum deposition temperature increases with an increase of $r(R^{3+})$. Below this temperature, the formation of additional *a*-axis-orientated crystallites in $RBa_2Cu_3O_{7-\delta}$ films was observed. This issue has already been exten-

(38) Locquet, J.-P.; Jaccard, Y.; Gerber, C.; Mächler, E. *Appl. Phys. Lett.* **1993**, *63*, 1426.

(39) Gnanasekar, K. I.; Sharon, M.; Pinto, R.; Pai, S. P.; Rao, M. S. R.; Apte, P. R.; Tamhane, A. S.; Purandare, S. C.; Gupta, L. C.; Vijayaraghavan, R. *J. Appl. Phys.* **1996**, *79*, 1082.

(40) Norton, D. P.; Lowndes, D. H.; Sales, B. C.; Budai, J. D.; Jones, E. C.; Chakoumakos, B. C. *Phys. Rev. B* **1994**, *49*, 4182.

(41) Samoylenkov, S. V.; Gorbenko, O. Yu.; Graboy, I. E.; Kaul, A. R.; Tretyakov, Yu. D. *J. Mater. Chem.* **1996**, *6*, 623.

(42) Samoylenkov, S. V.; Gorbenko, O. Yu.; Kaul, A. R.; Papucha, S. V.; Mirin, N. A.; Maleev, V. V.; Graboy, I. E.; Kuzhakhmetov, A. R.; Zhgoon, S. A. in: *Chemical Vapor Deposition*; Electrochemical Society Proceedings; 1997; Vol. 97−25, p 990.

(43) Jansen, J.; Tang, D.; Zandbergen, H. W.; Schenk, H. *Acta Crystallogr. A* **1998**, *54*, 91.

(44) Zandbergen, H. W.; Anderson, S. L.; Jansen, J. *Science* **1997**, *227*, 1221.

(45) Zandbergen, H. W.; Jansen, J. *J. Microscopy* **1998**, *190*, 222.

Table 2. Atomic Positions of $BaCu_3O_4$[a]

		X-ray diffraction of inclusions in $YBa_2Cu_3O_{7-\delta}$ single crystal,[57] room temperature			single crystal electron diffraction (this work), $T = 100$ K		
atom	position	*x*	*y*	*B*, Å^2	*x*	*y*	*B*, Å^2
Ba	0,0,0			0.60			0.8(1)
Cu(1)	$^1/_2$, $^1/_2$, $^1/_2$			0.45			0.2(1)
Cu(2)	x, 0, $^1/_2$	0.2979		0.60	0.248(9)		1.1(1)
O	x, y, $^1/_2$	0.1264	0.2543	0.91	0.127(1)	0.252(9)	1.6(1)

[a] Comparison between the data obtained by Bertinotti et al.[57] and from the refinement of single crystal electron diffraction along [100] and [010] zones of $BaCu_3O_4$ (this work).

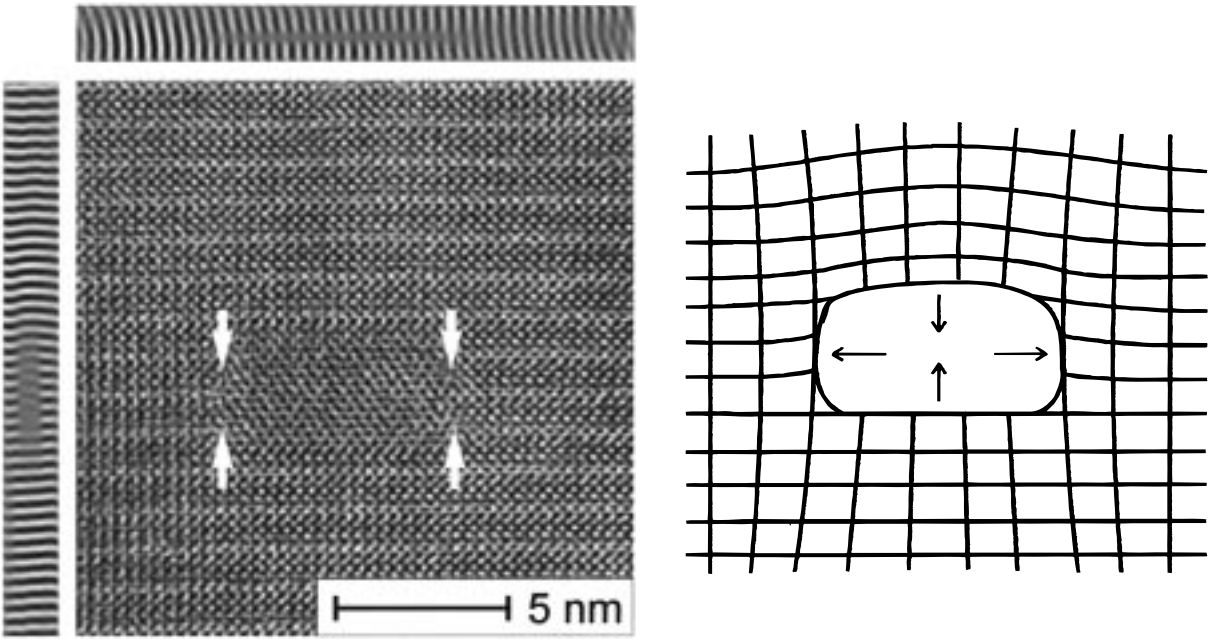

Figure 2. HREM image of Ho_2O_3 nanoinclusion in (001)$HoBa_2Cu_3O_{7-\delta}$ film along $[100]_{HoBCO}$. The bending of atomic planes of $HoBa_2Cu_3O_{7-\delta}$ (shown on the scheme) can be observed on Fourier transformed images compressed in the direction perpendicular to the atomic planes selected (above and to the left from the initial image) as well as four misfit dislocations (marked with white arrows).

sively discussed[42,46] and will not be addressed here. The variation of superconducting transition temperature and the *c* lattice parameter of $RBa_2Cu_3O_{7-\delta}$ films is in a accordance with the dependencies known for $RBa_2Cu_3O_{7-\delta}$ ceramics.[47−49] The critical current density j_c(77K,0T) decreases somewhat with the increase of $r(R^{3+})$. Unless otherwise stated, further discussion will concentrate on the range of $p(O_2)-T$ growth conditions limited by the values given in Table 1.

Secondary Phases Containing Rare Earth Cations. R_2O_3 secondary phases were detected by XRD in (001)$RBa_2Cu_3O_{7-\delta}$ (R = Lu, Ho) films on (001)$LaAlO_3$ and (001)$SrTiO_3$ substrates, if the film cation stoichiometry falls inside the $RBa_2Cu_3O_{7-\delta}-R_2O_3-CuO_x$ composition triangle (δ and *x* indexes are fixed for given deposition conditions) and the (001)-oriented $RBa_2Cu_3O_{7-\delta}$ phase is predominant in the film.

The formation of R_2O_3 inclusions for R = Lu[51] and Ho was confirmed by HREM (Figure 2). R_2O_3 inclusions were found either inside the $RBa_2Cu_3O_{7-\delta}$ film matrix or at the interface with the perovskite substrate. The inclusions normally had a platelike form with spatial dimensions in the [001] crystallographic direction in the 3.5−6 nm range for Ho_2O_3 and 5−12 nm for Lu_2O_3. The size of the inclusions in *ab* plane did not exceed 20 nm in both cases. Small dimensions of buried particles account for the broadening of (00*l*) reflections from R_2O_3 in XRD spectra (Figure 3). The following epitaxial relations were found:

$$(001)R_2O_3 \parallel (001)RBa_2Cu_3O_{7-\delta},\ [110]R_2O_3 \parallel [100]RBa_2Cu_3O_{7-\delta}$$

All these observations are very similar to those reported previously for epitaxial (001)$YBa_2Cu_3O_{7-\delta}$ films,[33−36] though another orientation has been also reported: (110)Y_2O_3 || (001)$YBa_2Cu_3O_{7-\delta}$, [001]Y_2O_3 || [100]$YBa_2Cu_3O_{7-\delta}$.[35,36]

(46) Kaul, A. R.; Molodyk, A. A.; Samoylenkov, S. V.; Markov, N. V.; Gorbenko, O. Yu.; Graboy, I. E.; Korsakov, I. E.; Wahl, G.; Stadel, O. In *NATO Science Series−3. High Technology*; Kluwer Academic Publishers: Dordrecht, 1999; Vol. 62, p 271.
(47) Lin, J. G.; Huang, C. Y.; Xue, Y. Y.; Chu, C. W.; Cao, X. W.; Ho, J. C. *Phys. Rev. B* **1995**, *51*, 12900.
(48) Williams, G. V. M.; Tallon, J. L. *Physica C* **1996**, *258*, 41.
(49) Chryssikos, G. D.; Kamitsos, E. I.; Kapoutsis, J. A.; Patsis, A. P.; Psycharis, V.; Koufoudakis, A.; Mitros, Ch.; Kallias, G.; Gamari-Seale, E.; Niarchos, D. *Physica C* **1995**, *254*, 44.
(50) Shannon, R. D. *Acta Crystallogr. A* **1976**, *32*, 751.
(51) Samoylenkov, S. V.; Gorbenko, O. Yu.; Graboy, I. E.; Kaul, A. R.; Svetchnikov, V. L.; Zandbergen, H. W. *Acta Phys. Polonica A* **1997**, *92*, 243.

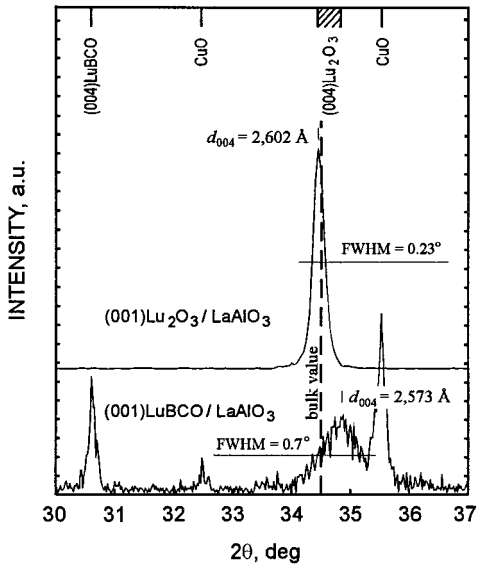

Figure 3. The contraction of the *c* axis of Lu_2O_3 inclusion in (001)$LuBa_2Cu_3O_{7-\delta}$ film matrix, as observed by XRD $\theta-2\theta$ scanning. The data for oriented Lu_2O_3/$LaAlO_3$ film are given for comparison (drawn not to scale). The dashed line denotes the position of the (004) reflection of bulk Lu_2O_3.

If no lattice relaxation is taken into account, the lattice mismatch between R_2O_3 and $RBa_2Cu_3O_{7-\delta}$ structures in the (001) plane (defined as $(a_m - a_i)/a_m$, where a_m and a_i are the lattice parameters of the film matrix and the inclusion) is equal to 4.2% and 2.6% for R = Lu and Ho, respectively. In the [001] direction, every third atomic layer of the R_2O_3 structure coincides with every fourth atomic layer of the $RBa_2Cu_3O_{7-\delta}$ structure with a mismatch of −0.2% for R = Lu and −2.8% for R = Ho. The misfit strain at the interface can be relaxed either through the formation of misfit dislocations or by distortion of neighboring unit cells. Our observations indicated that both mechanisms take place.

There are four misfit dislocations at the corners of a Ho_2O_3 inclusion. They can be clearly observed by viewing the image in Figure 2 along the direction of (013) planes of $HoBa_2Cu_3O_{7-\delta}$. Additionally, noticeable bending of atomic planes of the $HoBa_2Cu_3O_{7-\delta}$ matrix in the vicinity of the Ho_2O_3 inclusions can be observed after Fourier transformation of HREM images. The distortion is in agreement with the mismatch of corresponding structures. Accordingly, XRD analysis revealed the shortening of the lattice parameter of R_2O_3 inclusions in the direction normal to the interface plane (Figure 3). The *c* lattice parameters of Lu_2O_3 (Ho_2O_3) inclusions in $LuBa_2Cu_3O_{7-\delta}$ ($HoBa_2Cu_3O_{7-\delta}$) films were found to be scattered in 10.32−10.35 Å (10.50−10.56 Å) intervals, while the corresponding bulk values are 10.390 Å (10.606 Å). In contrast, the values of *c* lattice parameters for single-phase Ho_2O_3 and Lu_2O_3 in 0.1 μm thick films on (001)$LaAlO_3$ substrates grown under the same conditions were found to be very close to those of bulk materials: 10.40(1) and 10.61(1) Å, respectively (Figure 3).

Typical superconducting characteristics found for optimized (001)$HoBa_2Cu_3O_{7-\delta}$/$LaAlO_3$ films with a noticeable density of Ho_2O_3 inclusions (more than 0.5 mol %) were as follows: T_c in the range of 87−89K and j_c(77K,0T) of about 5×10^5−10^6 A/cm^2. These values are remarkably lower than those of stoichiometric films or films enriched with barium and copper (see Table 1). The structural disorder induced by the presence of embedded nanoparticles is probably the most important factor in lowering both T_c and j_c(77K).[52] The influence of Lu_2O_3 inclusions on superconducting properties of $RBa_2Cu_3O_{7-\delta}$ films was not so detrimental. In fact, (001)$LuBa_2Cu_3O_{7-\delta}$/$LaAlO_3$ sample with ca. 2.5 mol % of Lu_2O_3 impurity demonstrated excellent superconducting properties with T_c above 87 K and j_c(77K) higher than 2×10^6 A/cm^2. The smaller deformation of the superconducting matrix in the [001] direction resulting from the smaller lattice mismatch probably accounts for the lower sensitivity of $LuBa_2Cu_3O_{7-\delta}$ film properties to the presence of the Lu_2O_3 secondary phase.

In contrast to the lutetium and holmium systems, increasing the gadolinium content in the Gd−Ba−Cu−O system resulted in a gradual lowering of the *c* lattice parameter of the superconducting $GdBa_2Cu_3O_{7-\delta}$ phase without appearance of Gd_2O_3. T_c values of such films rapidly decreased from 90−91 K, the value typical for stoichiometric samples with a Gd:Ba concentration ratio about 1:2 and *c* parameter about 11.70−11.71 Å, reaching 83.5 K for the film with $c = 11.68$ Å. An attempt to grow a film with a large gadolinium excess led to the crystallization of a Gd_2CuO_4 secondary phase, with the superconducting matrix characterized by $c = 11.63$ Å. This behavior is similar to that reported recently for $NdBa_2Cu_3O_{7-\delta}$ thin films[53] and corresponds to the formation of $Gd_{1+x}Ba_{2-x}Cu_3O_{7-\delta}$ solid solutions. The decrease of the carrier concentration due to heterovalent substitution accounts for the decrease of T_c, as previously observed for $Nd_{1+x}Ba_{2-x}Cu_3O_{7-\delta}$[54] and $Sm_{1+x}Ba_{2-x}Cu_3O_{7-\delta}$[55] solid solutions in bulk.

In an excess of lutetium and copper, the oriented $Lu_2Cu_2O_5$ inclusions were also observed by HREM in our (001)$LuBa_2Cu_3O_{7-\delta}$ films.[21] $Lu_2Cu_2O_5$ phase nucleates only at the substrate surface, eventually forming large egglike inclusions of the size up to 0.2 μm. The epitaxial relations found by HREM for $Lu_2Cu_2O_5$ and $LaAlO_3$ were as follows:

$$[001]Lu_2Cu_2O_5 \parallel [011]LaAlO_3 \text{ and}$$
$$[013]Lu_2Cu_2O_5 \parallel [01\bar{1}]LaAlO_3$$

Finally, it should be mentioned that observations of (001)$YBa_2Cu_3O_{7-\delta}$ films were very similar to those of the holmium system described above. This similarity is expected due to the close values of the ionic radii of Ho^{3+} and Y^{3+} cations (see Table 1) and the resulting identity of the crystal chemistry and thermodynamics of holmium- and yttrium-related systems.

Secondary Phase Barium Cuprates in (001)RBa$_2$Cu$_3$O$_{7-\delta}$ Epitaxial Films. Depending on $p(O_2)-T$ conditions, $BaCuO_2$ or $BaCu_2O_2$ cuprates can exist in equilibrium with bulk $YBa_2Cu_3O_{7-\delta}$.[8−10] However, neither of these two phases was observed by XRD or TEM/HREM in our (001)$RBa_2Cu_3O_{7-\delta}$ epitaxial films. Instead, Ba_2CuO_{3+x} and $BaCu_3O_4$ formed when the film cation stoichiometry corresponded to the $RBa_2Cu_3O_{7-\delta}$−Ba_2CuO_{3+x}−$BaCu_3O_4$ or $RBa_2Cu_3O_{7-\delta}$−Ba_2CuO_{3+x}−

(52) Kawasaki, M.; Nantoh, M. *MRS Bull.* **1994**, *19*, 33.
(53) Kumagai, Y.; Yoshida, Y.; Iwata, M.; Hasegawa, M.; Sugawara, Y.; Hirayama, T.; Ikuhara, Y.; Hirabayashi, I.; Takai, Y. *Physica C* **1998**, *304*, 35.

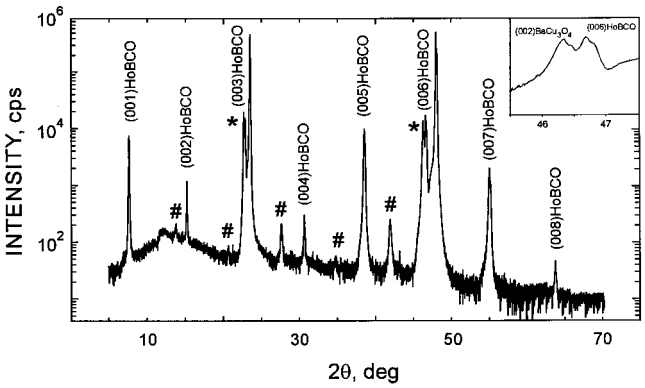

Figure 4. (00*l*) XRD peaks of Ba_2CuO_3 (marked with #, c = 12.92(3) Å) and $BaCu_3O_4$ (marked with *, c = 3.929(3) Å) secondary phases in (001)$HoBa_2Cu_3O_{7-\delta}$/$LaAlO_3$ film with Ho:Ba:Cu cation stoichiometry 8.9:30.4:60.7 (EDX data). Inset: magnified $\theta-2\theta$ diffraction pattern of (002)$BaCu_3O_4$ and (006)$HoBa_2Cu_3O_{7-\delta}$ reflections.

CuO_z composition triangles (δ, x, and z are constant), respectively. An XRD $\theta-2\theta$ scan for a (001)$HoBa_2Cu_3O_{7-\delta}$/$LaAlO_3$ film containing (001)-oriented Ba_2CuO_{3+x} and $BaCu_3O_4$ impurities is shown in Figure 4.

Ba_2CuO_{3+x} is known to possess an anion-deficient K_2NiF_4 type structure[56] with a wide range of oxygen nonstoichiometry.[16] The orthorhombic lattice parameters of Ba_2CuO_{3+x} (x = 0) were reported by Wong-Ng et al.:[56] a = 3.9069(5) Å, b = 4.1007(3) Å, and c = 12.9655(14) Å. The phase observed in our samples was (001)-oriented, which could be expected from the values of the a and b lattice parameters, allowing good lattice matching with the (001) plane of $RBa_2Cu_3O_{7-\delta}$. The value of the c lattice parameter observed, 12.92(3) Å, was in agreement with that reported in ref 56. The same value for the lattice parameter c was found for single-phase (001)-oriented Ba_2CuO_{3+x} films grown on (001)-$LaAlO_3$ and (001)$SrTiO_3$ substrates under the same deposition conditions. Ba_2CuO_{3+x} samples, however, were extremely unstable in air, making their analysis rather troublesome.

$BaCu_3O_4$ is absent in all Ba−Cu−O phase diagrams reported to date. To the best of our knowledge, there has been only one report on the observation of $BaCu_3O_4$. Namely, Bertinotti et al.[57] observed $BaCu_3O_4$ as perfectly oriented secondary phase inclusions in $YBa_2Cu_3O_{7-\delta}$ single crystals and refined its structure and composition from single-crystal XRD experiments. $BaCu_3O_4$ possesses the orthorhombic layered structure with lattice parameters a = 10.986(3) Å, b = 5.503(1) Å, c = 3.923(1) Å. The lattice parameters derived from XRD measurements of our film samples are in good agreement with these results: a = 11.01(2) Å, b = 5.50(1) Å, c = 3.923(2) Å.

To establish the composition of the phase observed as that of $BaCu_3O_4$, a series of 0.2 μm thick Ba−Cu−O films with varying ratios of barium and copper content were deposited on (001)$LaAlO_3$ substrates at 815 °C and $p(O_2)$ = 1.7 mbar. For single phase $BaCu_3O_4$ films, the Ba:Cu atomic ratio determined by EDX was equal to 1:3. With an excess of copper or barium, CuO or Ba_2CuO_{3+x} secondary phases respectively appeared. The perfect alignment of the $BaCu_3O_4$ was found. Pole figures taken for the (111) reflection of $BaCu_3O_4$ grown on (001)$LaAlO_3$ and (001)$SrTiO_3$ substrates revealed two types of orientations (with twins):

(001) $BaCu_3O_4$ || (001)ABO_3, [210] $BaCu_3O_4$ || [100]ABO_3 and [210] $BaCu_3O_4$ || [010]ABO_3

(210) $BaCu_3O_4$ || (001)ABO_3, [001] $BaCu_3O_4$ || [100]ABO_3 and [001] $BaCu_3O_4$ || [010]ABO_3

where ABO_3 denotes either $LaAlO_3$ or $SrTiO_3$ (Figure 5). For both (001) and (210) orientation of $BaCu_3O_4$, the resulting lattice mismatch at the interface plane is 3% and 0.5% for $LaAlO_3$ and $SrTiO_3$ substrates, respectively.

There remains a question whether the $BaCu_3O_4$ phase could appear in $RBa_2Cu_3O_{7-\delta}$ films prepared by other deposition techniques, e.g. PLD or magnetron sputtering, or not. The main analytical problem is the proximity of d_{001} and d_{210} of $BaCu_3O_4$ to the c/3 parameter of $RBa_2Cu_3O_{7-\delta}$ (see Figure 4, inset), which makes its identification rather difficult. Actually, the content of the $BaCu_3O_4$ phase must be rather large for an unambiguous decision to be made on the basis of XRD data.

The stabilization of $BaCu_3O_4$ as a thin film and as a secondary phase in epitaxial (001)$RBa_2Cu_3O_{7-\delta}$ films is strongly connected with its oriented growth. To investigate the subject in more detail, 0.2 μm thick Ba−Cu−O films (with Ba:Cu concentration ratio about 1:3) on (001)$SrTiO_3$ and (110)$SrTiO_3$ substrates were prepared in a single deposition run. The results of an XRD analysis show that the $BaCu_3O_4$ phase does not form on (110)$SrTiO_3$ substrates. Instead, the formation of randomly oriented $Ba_2Cu_3O_{5+y}$ and CuO phases was observed (Figure 6). No XRD reflections were observed also for 0.2 μm thick Ba−Cu−O film (Ba:Cu 1:3) on (001)MgO substrate. In this case, the large lattice mismatch between MgO and $BaCu_3O_4$ (about 7% in the ab plane) prohibits the nucleation of the latter.

The orientation-induced stabilization was found to depend on $BaCu_3O_4$ film thickness. In Figure 7 the normalized XRD intensities of the constituting phases are plotted against the average film thickness for several Ba−Cu−O samples (Ba:Cu 1:3). XRD peaks of $BaCu_3O_4$ increase in intensity with the film thickness, until at some critical value of ca. 0.3 μm a sudden drop in intensity occurs. On the other hand, peaks corresponding to phases thermodynamically stable in bulk, i.e., $BaCuO_2$ and CuO,[16] take over at this critical film thickness and rapidly increase in intensity with increasing thickness. Thus, decomposition of $BaCu_3O_4$ takes place in films thicker than ~0.3 μm according to the reaction:

$$BaCu_3O_4 \rightarrow BaCuO_2 + 2CuO \quad \text{(reaction 1)}$$

The surface morphology of two films, a nearly single-phase thin $BaCu_3O_4$ film, and a thicker film consisting mainly of polycrystalline CuO and $BaCuO_2$, are shown

(54) Kramer, M. J.; Yoo, S. I.; McCallum, R. W.; Yelon, W. B.; Xie, H.; Allenspach, P. *Physica C* **1994**, *219*, 145.
(55) Plackowski, T.; Sulkowski, C.; Bukowski, Z.; Wlosewicz, D.; Rogacki, K. *Physica C* **1995**, *254*, 331.
(56) Wong-Ng, W.; McMurdie, H. F.; Paretzkin, B.; Hubbard, C. R.; Dragoo, A. L. *Powder Diffraction* **1988**, *3*, 113.
(57) Bertinotti, A.; Hamman, J.; Luzet, D.; Vincent, E. *Physica C* **1989**, *160*, 227.

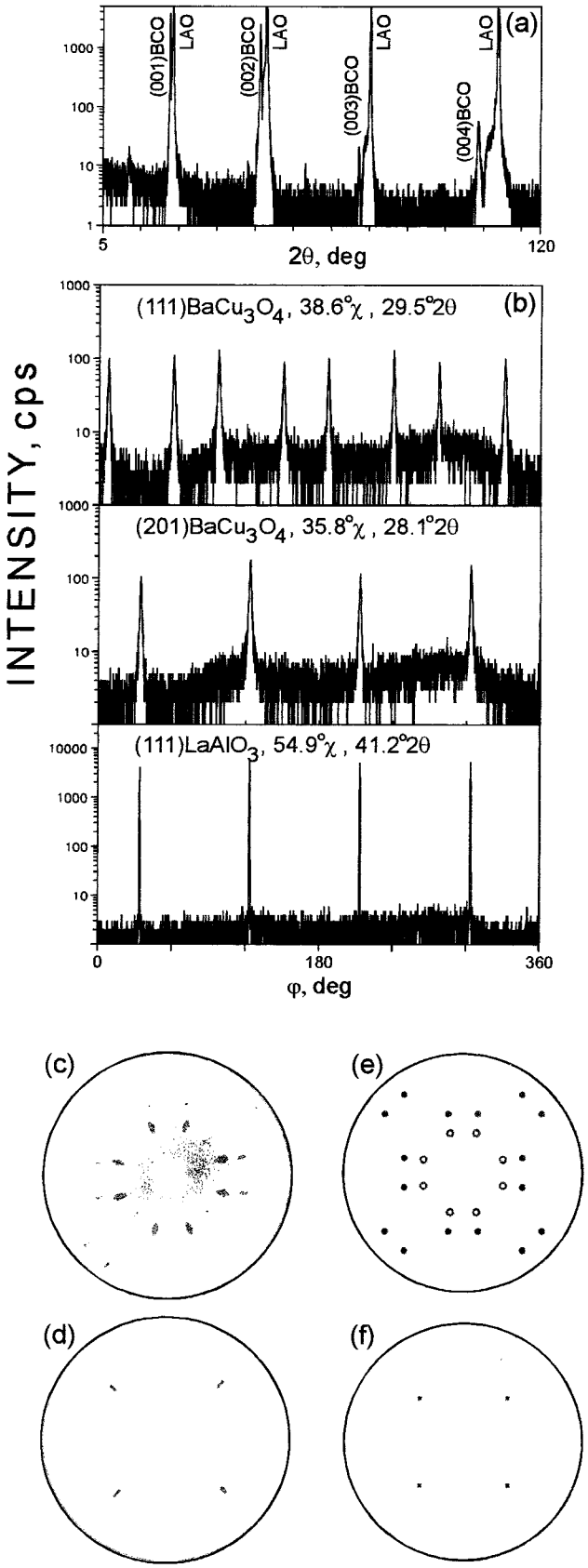

Figure 5. XRD analysis of single-phase $BaCu_3O_4$ film on $LaAlO_3$ substrate. (a) $\theta-2\theta$ scan, (b) φ scans, (c, d) pole figures of the (111) reflections of $BaCu_3O_4$ and $LaAlO_3$, respectively. (e, f) the calculated pole figures [on the pole figure of $BaCu_3O_4$, open circles denote (001) orientation, closed circles denote (210) orientation].

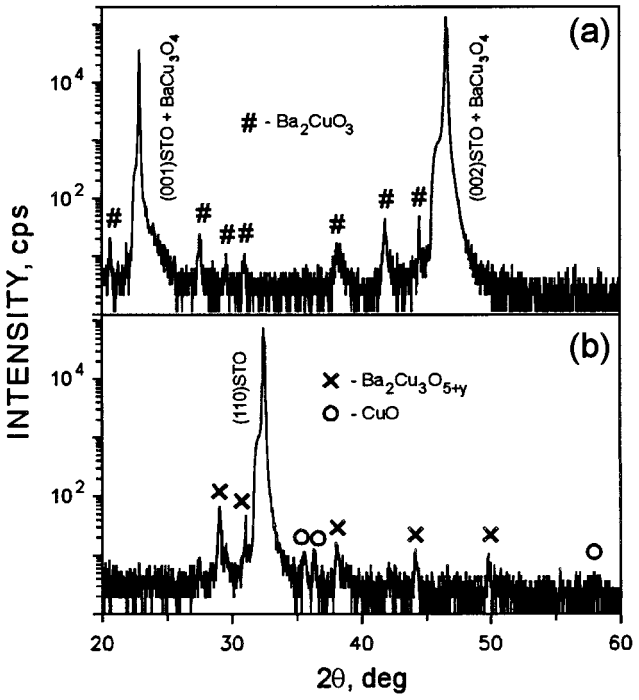

Figure 6. XRD $\theta-2\theta$ scans of Ba−Cu−O films (Ba:Cu concentration ratio is about 1:3) deposited on (001)$SrTiO_3$ (a) and (110)$SrTiO_3$ (b) substrates.

in Figure 8. The epitaxial $BaCu_3O_4$ phase grows in the form of partly cornered islands of about 1 μm in size (Figure 8a). This morphology was found to be rather typical; in fact, we could not prepare $BaCu_3O_4$ films with dense coverage of the substrate surface. It is reasonable to assume the presence of liquid phases in the multiphase thick film (Figure 8b), which can promote the further decomposition of $BaCu_3O_4$ and account for the decrease of intensity of $BaCu_3O_4$ XRD peaks (Figure 7).

To study a possible oxygen nonstoichiometry of the compound, we undertook annealings on $BaCu_3O_4$ films under oxidizing and reducing conditions. The lattice parameter *c* of the as-grown film was not influenced by the annealing in argon flow ($p(O_2) \sim 0.1$ mbar) at 800 °C for 1 h, nor by the annealing in oxygen while the temperature was gradually decreased from 550 to 150 °C in 4 h. Therefore, it is rather possible that $BaCu_3O_4$ possesses no significant oxygen nonstoichiometry, at least under the conditions used.

HREM and Electron Diffraction Structure Analysis of $BaCu_3O_4$. HREM investigation of $BaCu_3O_4$ inclusions has been performed on the epitaxial (001)-$HoBa_2Cu_3O_{7-\delta}$/(001)$LaAlO_3$ film containing about 60 mol % of $BaCu_3O_4$ phase according to EDX analysis. The $BaCu_3O_4$ particles were observed exclusively on the films surface in a well-oriented form. The interface between $BaCu_3O_4$ and $HoBa_2Cu_3O_{7-\delta}$ phases was found to be rather sharp and free from impurity phases (Figure 9). However, a high defect density was observed in the layers of $HoBa_2Cu_3O_{7-\delta}$ material close to the interface.

For the structure refinement, a number of diffraction patterns were recorded from $BaCu_3O_4$ crystallites in [100] and [010] orientations. A typical diffraction pattern is shown in Figure 10. A misorientation of the crystal is evident from the asymmetry of the diffraction spots around the central spot. A larger misorientation

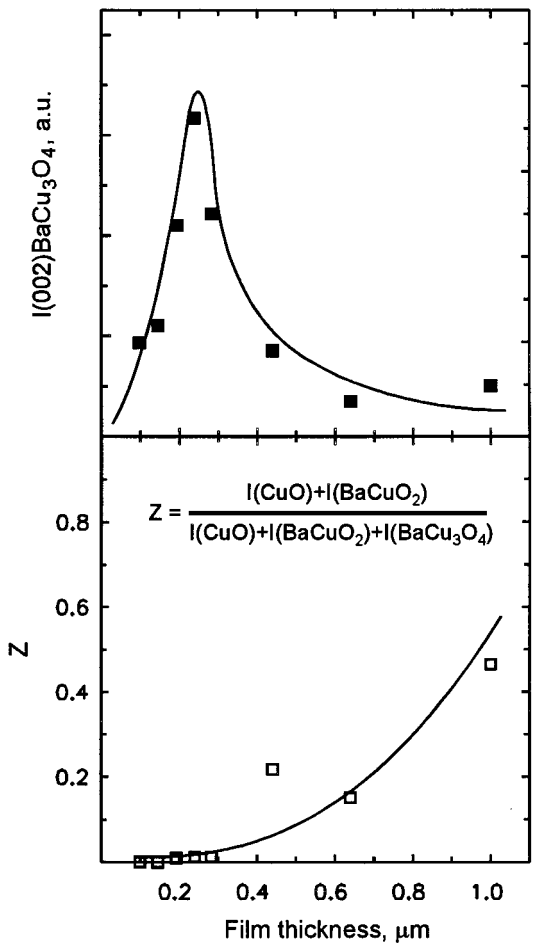

Figure 7. The variation of the intensity of $BaCu_3O_4$ (002) XRD peak (upper graph) and normalized intensities of polycrystal reflections of CuO and $BaCuO_2$ vs the thickness of the deposited film.

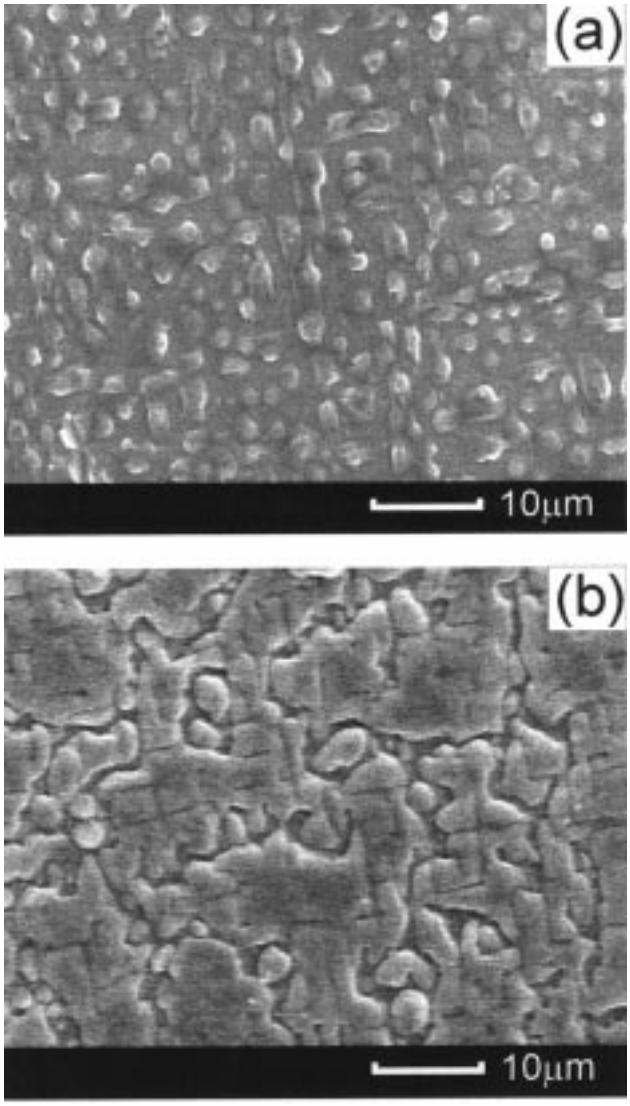

Figure 8. SEM images the surface morphology of 0.18 μm (a) and 0.63 μm (b) thick $BaCu_3O_4$ films on $LaAlO_3$ substrate. Note the island type growth of the thin film and the meltlike surface of the thick one.

results in fewer diffraction spots on the side where they are already weak and an increase in the high-order reflections on the other side, such that even reflections with *g*-values well below 0.05 nm can be significant.

Fourteen data sets taken from areas with a range of thicknesses 4−16 nm were used for the refinement to increase the accuracy of the determination of the atomic parameters. Since only [100] and [010] diffraction patterns are used, there is a strong correlation of the *x* parameter of Cu(2) with its thermal parameter *B* and the *y* parameter of O with its *B* parameter. Because of this correlation the refinement was first executed with an overall *B* value. Next, the individual *B* parameters were refined with fixed *x*(Cu(2)) and *y*(O). Finally, a single cycle was made in which all parameters were refined. The refinements of possible O positions in the $z = 0$ plane, containing barium atoms, indicated that no significant amount of oxygen is present in this plane. The results of the MSLS refinement with an overall *R* value of 3.6% (3.8% for all reflections) are listed in Table 2. Comparison of the atomic parameters obtained from the MSLS software and those obtained by Bertinotti et al.[57] shows quite a good agreement.

The structure of $BaCu_3O_4$ is shown in Figure 11. $BaCu_3O_4$ can be regarded as a member of the $A_{n-1}Cu_{n+1}O_{2n}$ homologue family (A = alkaline earth element). Previously, $Sr_{n-1}Cu_{n+1}O_{2n}$ cuprates with $n = 3$, 5, 7, and 9 (spin ladder compounds) and $n =$ infinity (infinite layers) have been synthesized under high pressure.[58] The barium cuprate observed in our work can be referred to as the member of the Ba−Cu−O family with $n = 2$.

CuO and Cu_2O Secondary Phases. CuO and Cu_2O phases are known to exist in equilibrium with $RBa_2Cu_3O_{7-\delta}$ phases over a wide range of $p(O_2)-T$ conditions, including those used in the present work.[7−9] The actual copper oxide composition depends on the conditions of sample cooling; the conditions used in our work always led to the formation of CuO.

Large CuO particles, of about 1 μm in size, were observed on the surface of $(001)RBa_2Cu_3O_{7-\delta}$ films (Figure 12). The distances between neighboring particles were often found to be rather large, sometimes even exceeding several tens of microns. TEM of the films' cross sections showed that CuO particles are located on the surface of the epitaxial film and very rarely reside

(58) Hiroi, Z.; Takano, M. *Physica C* **1994**, *235−240*, 29, and references within.

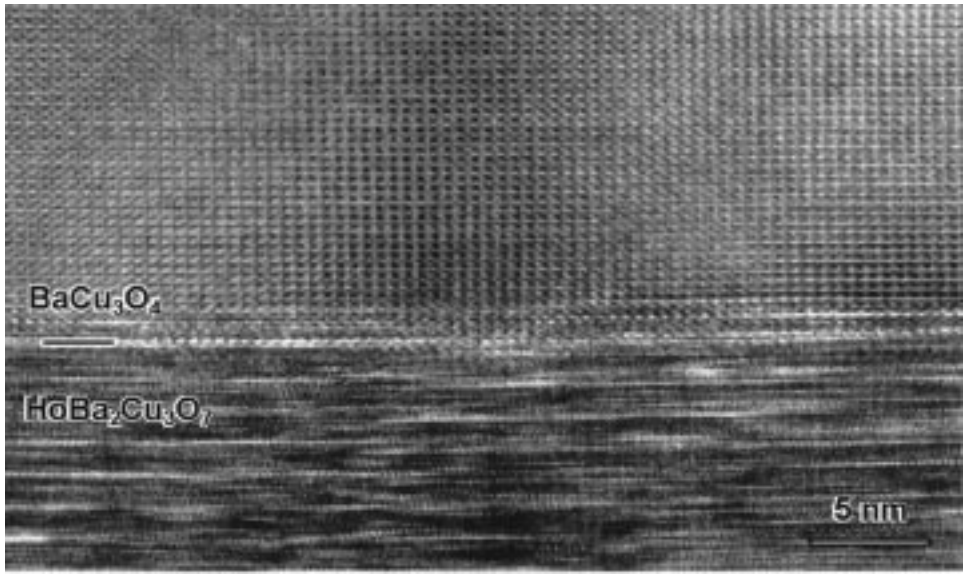

Figure 9. HREM image of the $BaCu_3O_4/HoBa_2Cu_3O_{7-\delta}$ interface along $[110]_{HoBCO}$, whereas $BaCu_3O_4$ is in [010] orientation. The interface is sharp and shows no additional phases. *c* axes of $BaCu_3O_4$ and $HoBa_2Cu_3O_{7-\delta}$ are parallel.

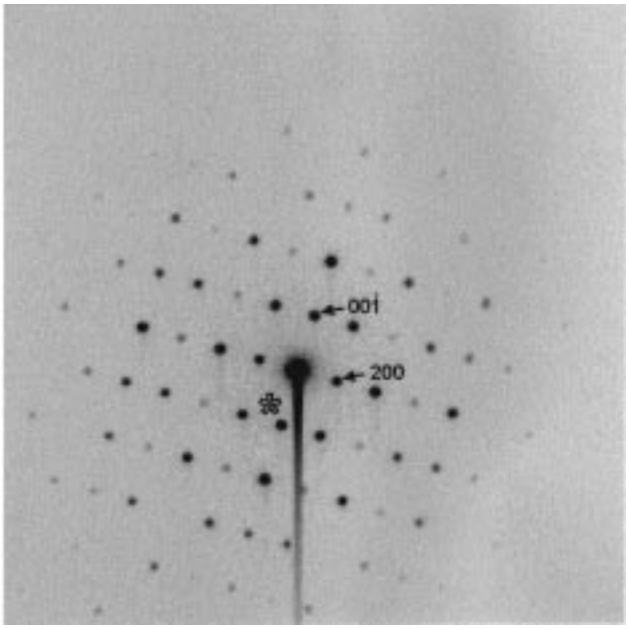

Figure 10. An example of the recorded electron diffraction pattern of [010]-oriented $BaCu_3O_4$. The 0,0,0 beam is the strongly overexposed spot. Due to the overexposure and the way the CCD is read out, a streak is created through this 0,0,0 spot. A few diffraction spots are also overexposed, resulting in similar streaks. The calculated center of the Laue circle is indicated by an asterisk. Several observed spots are indicated. The $\underline{1}600$ reflection corresponds to a *d*-spacing of 0.058 nm. Due to the misorientation of the crystal, the visibility of the reflections continues much further on the left side of the 0,0,0 spot.

inside the (001)$RBa_2Cu_3O_{7-\delta}$ matrix. This behavior is consistent with that reported previously for (001)$YBa_2Cu_3O_{7-\delta}$ epitaxial films.[38,52] The surface of $RBa_2Cu_3O_{7-\delta}$ films near CuO particles was found to be remarkably smoother, as compared to that far from precipitates. Finally, we observed that the presence of a small quantity of excess copper in $RBa_2Cu_3O_{7-\delta}$ films was quite favorable, as far as the films epitaxial quality and superconducting characteristics were concerned.

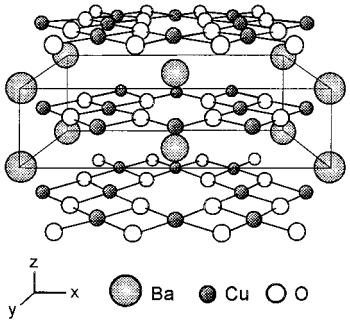

Figure 11. The structure of $BaCu_3O_4$. Note, that it consists of alternating Cu_3O_4 layers and oxygen-free Ba layers.

IV. Discussion

All the secondary phases observed in our (001)$RBa_2Cu_3O_{7-\delta}$ films, except for CuO, are believed to exist in *nonequilibrium* with bulk $RBa_2Cu_3O_{7-\delta}$. Nevertheless, *being well-oriented*, all these phases can coexist with the epitaxial $RBa_2Cu_3O_{7-\delta}$ matrix, forming coherent or semicoherent grain boundaries with it. Thus, the structure and orientation of the growing film can govern to a great extent the appearance of particular phases, depending on the resemblance of their crystal structures to the structure of the film matrix. Consequently, those growth parameters which affect in the film epitaxial quality (e.g. substrate structure and orientation) turned out to be very important factors in determining the phase composition of the deposited material. Let us discuss the origin of this behavior in some more detail.

For the formation of a secondary phase inclusion in a matrix of another compound, the following expression of the Gibbs' energy can be written

$$\Delta G_f = \Delta g^{vol} V + \sigma S + \Delta G^{stress} \qquad (1)$$

where $\Delta g^{vol} V$ and σS are the Gibbs' energies corresponding to the volume of the inclusion (V) and the interface with the matrix over area (S), respectively. For a thermodynamically stable phase, $\Delta g^{vol} < 0$. The value of σ is always positive, denoting the increase in the system's energy corresponding to the formation of the

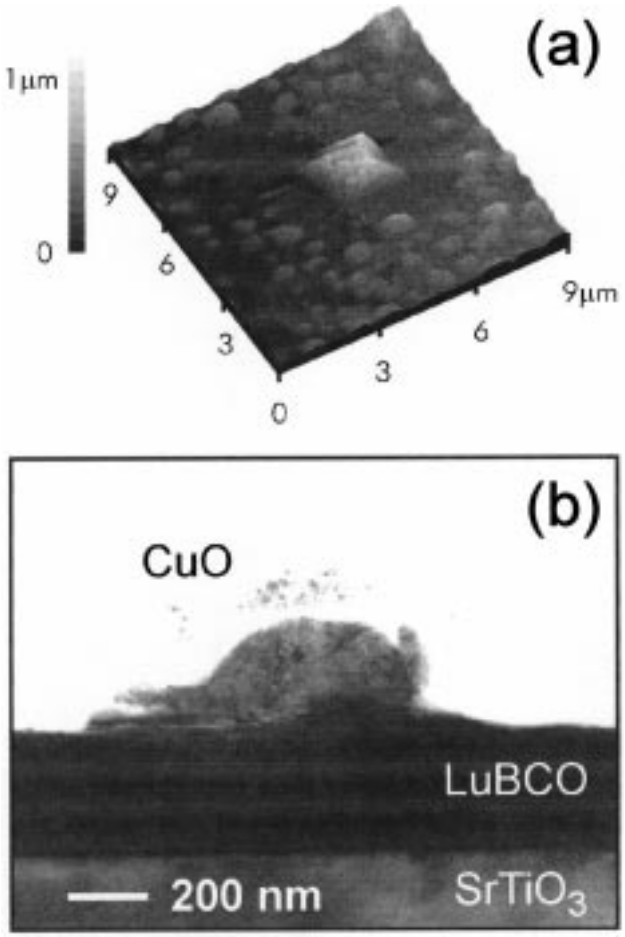

Figure 12. CuO particle on the surface of the (001)$LuBa_2Cu_3O_{7-\delta}$ film: AFM (a) and TEM (b) images.

interface. The last term, ΔG^{stress}, accounts for the change of bulk and interface energies of the system due to the lattice strain induced by the presence of the foreign inclusion in the film matrix. Equation 1 could be alternatively written with only two terms on the right side, which correspond to the *strained* state of the inclusion and the matrix:

$$\Delta G_f = \Delta G^{vol} + \Delta G^{int} \qquad (2)$$

The interface term ΔG^{int} dominates over ΔG^{vol} when the dimension of the inclusion d is small enough. The nucleus of the phase is thermodynamically stable only for d exceeding some critical value, d^{cr}. The activation energy barrier E_a must be overcome for a nucleus of a critical size to be formed (Figure 13). The coherent and semicoherent interfaces correspond to relatively low values of d^{cr} and E_a, while relatively large d^{cr} and E_a values are typical for incoherent interfaces. The imaginary grain boundary in the perfect crystal with $\Delta G^{int} = 0$ results in $d^{cr} = E_a = 0$, while a free crystal surface results in the largest possible ΔG^{int}, d^{cr}, and E_a values. Due to the significance of the interface term, the type of nucleating secondary phase can vary, depending on the possibility of the formation of coherent or semicoherent interfaces with the surrounding matrix. In particular, an inclusion of a nonequilibrium-in-bulk phase could turn out to be more stable than an inclusion of an equilibrium phase, if the latter can form only high-energy grain boundaries with the matrix (Figure 13).

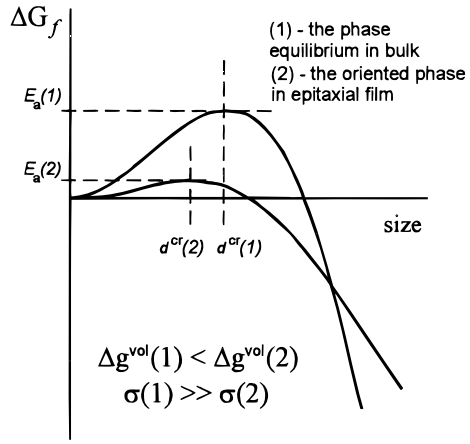

Figure 13. Gibbs' formation energy of the secondary phase inclusions in the epitaxial matrix vs the inclusion size. Note, that the formation of the coherent inclusion of the nonequilibrium in bulk phase can be more favorable, if the inclusion size is small enough.

This kind of stabilization corresponds to the supposition c in the Introduction to this article.

The significant role of the interface term is quite feasible, since the values of the Gibbs's energy for solid-state exchange reactions of complex oxides are usually very moderate. The following values are calculated using thermodynamic data reported in refs 9, 59, and 60 for the reaction of interest (T = 820 °C, $p(O_2)$ = 1 mbar):

$$^1/_2Y_2O_3 + {}^1/_3YBa_2Cu_3O_{6.08} + 0.07O_2 \leftrightarrow {}^2/_3Y_2BaCuO_5 + {}^1/_3CuO$$
$$\Delta G_r = -10\ 104\ \text{kJ} \quad \text{(reaction 2)}$$

As it was mentioned above, the typical size of R_2O_3 inclusions observed did not exceed some 10 nm. For Y_2O_3 inclusion of a typical size, 12 × 12 × 6 nm^3, according to reaction 2 the excess volume energy is ~4 × 10^{-16} J. The gain in the interface energy needed to compensate for this value roughly equals 700 mJ/m^2. The energy of incoherent interfaces should approach the values typical for a free crystal surface, which are known to be on the order of 1−3 J/m^2 for oxides.[61,62] At the same time, the energy of coherent or semicoherent interfaces can be lower by a factor of 2 or 3 than the value of the incoherent interfaces.[63] Thus, the typical interface energy gain may be large enough to shift equilibrium 2 in favor of formation of oriented Y_2O_3 inclusions, instead of nonoriented inclusions of the Y_2BaCuO_5 phase. The strain energy terms of eq 1 should not differ significantly from each other for the formation of either Y_2O_3 or Y_2BaCuO_5 inclusions. Therefore, the strain of the crystal lattice can hardly significantly destabilize Y_2O_3 inclusions in the $YBa_2Cu_3O_{7-\delta}$ film matrix. Unfortunately, more accurate numerical analy-

(59) Degterov, S. A.; Voronin, G. F. *Superconductivity* **1991**, *4*, 765 (in Russian).
(60) Degterov, S. A.; Voronin, G. F. *Superconductivity* **1991**, *4*, 1758 (in Russian).
(61) Mileto Ganozio, F.; Scotti di Uccio, U. *J. Cryst. Growth* **1997**, *174*, 409.
(62) Rehbein, C.; Michel, F.; Harison, N. M.; Wander, A. *Surf. Rev. Lett.* **1998**, *5*, 337.
(63) Sutton, A. P.; Balluffi, R. W. *Interfaces in Crystalline Materials*; Calendron Press: Oxford, 1995.

sis of interface and stress energies is extremely complex, and only for metals or ionic compounds with a simple structure reliable data are available.

Due to a large difference in crystal structures, no reasonable lattice match of R_2BaCuO_5 and $RBa_2Cu_3O_{7-\delta}$ structures is possible and R_2BaCuO_5 secondary phase does not nucleate in (001)$RBa_2Cu_3O_{7-\delta}$ epitaxial films. Instead, semicoherent nanoinclusions of nonequilibrium-in-bulk R_2O_3 (R = Lu,Ho,Y) phases did form. The interfaces observed (Figure 2) did not contain any impurity phases which could be attributed to a chemical interaction between R_2O_3 and $RBa_2Cu_3O_{7-\delta}$, even though under the film growth conditions used diffusion is expected to be fast enough for any possible chemical reactions to proceed. Following these considerations, we suggest that thermodynamical equilibrium exists between oriented R_2O_3 and $RBa_2Cu_3O_{7-\delta}$ phases in films, i.e., the equilibrium phase relations are different for bulk ceramics and epitaxial films.

In sharp contrast, the Gd_2O_3 secondary phase was not observed in (001)$GdBa_2Cu_3O_{7-\delta}$ epitaxial films by HREM or by XRD. The absence of the Gd_2O_3 secondary phase in epitaxial (001)$GdBa_2Cu_3O_{7-\delta}$ films is probably due to the formation of $Gd_{1+x}Ba_{2-x}Cu_3O_{7-\delta}$ solid solutions and Gd_2CuO_4 secondary phase. The latter possesses a good lattice match with the $GdBa_2Cu_3O_{7-\delta}$ structure and appears in a highly oriented form. Besides that, the stability of R_2O_3 oxides with cubic C-type structure decreases with the increase of $r(R^{3+})$[64] and this is another possible reason for the absence of Gd_2O_3 secondary phase in epitaxial (001)$GdBa_2Cu_3O_{7-\delta}$ films.

Thus, the formation of the R_2O_3 secondary phase inclusions becomes more unfavorable as $r(R^{3+})$ increases—the critical value of the ionic radius is expected to be between those of holmium and gadolinium. This observation is in accordance with the various literature data. To the best of our knowledge, there has been only one report discussing Gd_2O_3 phase formation in $GdBa_2Cu_3O_{7-\delta}$ films.[65] In that case, however, nanoparticles of gadolinium oxide were not formed inside the (001)$GdBa_2Cu_3O_{7-\delta}$ matrix, but close to other structural defects such as (100)-oriented grains of $GdBa_2Cu_3O_{7-\delta}$.

We believe that the same considerations are applicable to all oriented phases observed in our films. Though the thermodynamic stability of $BaCu_3O_4$ in epitaxial films could be argued, we have not observed any signs of its decomposition, even after annealing at 800 °C, $p(O_2) \sim 0.1$ mbar, for 1 h. This observation indicates that the stabilization effect can hardly be kinetic in origin. It is more likely that the stability of $BaCu_3O_4$ in epitaxial thin films is due to the similarity of its structure with that of the perovskite substrate or $RBa_2Cu_3O_{7-\delta}$ causing the formation of oriented nuclei stabilized by the lowered energy of a coherent interface. Changes in the substrate orientation or the lattice mismatch makes the formation of a coherent low-energy interface no longer possible and prohibits $BaCu_3O_4$ nucleation. Accordingly, the increase of the size of the $BaCu_3O_4$ crystallites should make them less stable as compared to thermodynamically stable-in-bulk $BaCuO_2$ and CuO (Figure 13). Therefore, the decomposition of $BaCu_3O_4$ according to reaction 1 takes place with the film thickness increasing over some critical value (Figure 7).

Our results are consistent with observations of $BaCu_3O_4$ as a perfectly oriented secondary phase in $YBa_2Cu_3O_{7-\delta}$ single crystals.[57] The growth of $YBa_2Cu_3O_{7-\delta}$ single crystals from a melt takes place for a rather prolonged time at a higher temperature and lower supersaturation levels, compared to thin film growth. According to this, single crystalline materials are usually well-equilibrated. This is another argument to suppose the thermodynamic stability of $BaCu_3O_4$ in an epitaxial state.

Among the secondary phases described in this report, CuO and $BaCu_3O_4$ were shown to appear exclusively on the films' surface as particles of about 1 μm in size. No evidence of the presence of CuO and $BaCu_3O_4$ inside $RBa_2Cu_3O_{7-\delta}$ matrix have been observed by HREM. The behavior was clearly observed even for quite large amounts of these secondary phases in films (e.g. for 60 mol % of $BaCu_3O_4$ in $HoBa_2Cu_3O_{7-\delta}$ film), which makes their formation at the late stages of the growth or during the cooling unlikely. It is noteworthy that, while $BaCu_3O_4$ secondary phase is present in $RBa_2Cu_3O_{7-\delta}$ films only due to its perfect lattice match with the matrix, CuO particles are usually not oriented. Thus, a poor lattice match cannot be the main reason accounting for residence of the particles on the surface, as it was assumed in our earlier work.[21] It is more likely that the migration of CuO or $BaCu_3O_4$ to the film surface takes place due to enhanced diffusion along the interface between the inclusion and the $RBa_2Cu_3O_{7-\delta}$ matrix. The relatively low melting points of the eutectics formed by $RBa_2Cu_3O_{7-\delta}$ with CuO and/or barium cuprates could cause this diffusion enhancement. Effective mass transport along the interface allows for a rapid film growth even beneath the particle, so that the particle is eventually pushed onto the films surface. The observed smoothening of the films' surface near CuO particles indicates the existence of intensive surface diffusion flux in a copper-rich region. An alternative explanation suggests a high mobility of the secondary phase particles on the film surface during the growth.

In contrast, R_2O_3 oxides and eutectics with them possess the highest melting points in R−Ba−Cu−O systems, so the diffusion along the interface between the R_2O_3 and $RBa_2Cu_3O_{7-\delta}$ phases is expected to be relatively slow. Accordingly, R_2O_3 inclusions were observed exclusively inside the film matrix, or at the film/substrate interface. In contrast to large particles of CuO and $BaCu_3O_4$, the size of R_2O_3 inclusions in $RBa_2Cu_3O_{7-\delta}$ films rarely exceeds 20 nm in the (001) crystallographic plane, while their density can be quite high. Evidently, slow diffusion of triple-charged rare earth cations makes rapid growth of R_2O_3 particles and their migration onto the film surface impossible. This observation is in accordance with the nucleation scheme of Y_2O_3 precipitates in $YBa_2Cu_3O_{7-\delta}$ films presented in ref 36.

V. Conclusions

The phase relations of complex oxide systems in thin epitaxial films may differ from those known for bulk materials. In this study, the formation of nonequilibrium-in-bulk phases and the appearance of new phase

(64) Roth, R. S.; Schneider, S. J. *J. Res. NBS* **1960**, *64A*, 390.
(65) Li, Y. H.; Staton-Bevan, A. E.; Kilner, J. A. *Physica C* **1996**, *257*, 382.

relations has been observed in off-stoichiometric epitaxial (001)$RBa_2Cu_3O_{7-\delta}$ films. It was supposed that the formation of coherent interfaces, which are inherent in epitaxial film growth, enables stabilization of otherwise nonequilibrium phases. For instance, epitaxial growth of a new barium cuprate, $BaCu_3O_4$, has been demonstrated on (001) single crystalline perovskite substrates, and its structure has been refined using electron nanodiffraction of the films' cross sections.

Contemporary thin film growth techniques provide a powerful tool for synthesis of unstable-in-bulk compounds in an epitaxial state. Up to now, the stabilization due to kinetical reasons has been intensively studied for thin films of complex oxides (e.g. MBE synthesis of artificial structures[66]). The observations presented in this work show that thermodynamic stabilization due to the lowered energy of coherent interfaces can be also possible and point to thin film epitaxy as an indispensable tool in the search for new complex oxides.

Acknowledgment. INTAS-RFBR (grant IR 97-1954), Copernicus program (grant ERBIC15CT-960735), VW Project I/73628, Stichting Fundamenteel Onderzoek der Materie, and the European Commission (contract ERMRXCT 98-0189) are acknowledged for financial support.

CM991016V

(66) Balestrino, G.; Martellucci, S.; Medaglia, P. G.; Paoletti, A.; Petrocelli, G. *Physica C* **1998**, *302*, 78.